HIGH GAIN CIRCULARLY POLARIZED ANTENNA WITH A SUPERSTRATE LAYER FOR AEROSPACE COMMUNICATION

Luiza Leszkowska [(1)], Mateusz Rzymowski [(1)], Lukasz Kulas [(1)], Krzysztof Nyka [(1)]

[(1)] Department of Microwave and Antenna Engineering, Faculty of Electronics, Telecommunications and Informatics, Gdansk University of Technology, ul. Narutowicza 11/12, 80-233 Gdansk, Poland, {luiza.leszkowska, mateusz.rzymowski, lukasz.kulas, krzysztof.nyka}@pg.edu.pl

ABSTRACT

In this paper, the concept of a low-cost circularly polarized antenna with partially reflecting surface (PRS) has been adopted for point-to-point connectivity in aerospace communication. The investigation contains an analysis of dependence of the antenna performance on elements number in the PRS structure which allows establishing a compromise between the overall size of the antenna and its gain, the parameters that are significant especially from the perspective of small satellites. For this purpose, X- and Ka-band frequencies, which provide high throughput and are widely used in satellite communications, were chosen to generate simulation results of the antenna and investigate its gain, circular polarization, efficiency and key physical requirements – lightweight and compact size. It has been shown that satisfactory antenna parameters can be achieved for overall size of 65 *x* 65 *x* 23 mm and 30 *x* 30 *x* 7 mm in X band and Ka band, respectively. The best antenna designs that may be used in Cubesat, UAV or HAPS communication links have been fabricated and measured to validate the proposed approach and designs. It has shown that such universal antennas can seamlessly be implemented in aerospace communication systems in which different platforms (i.e. Cubesat, UAV or HAPS) have to collaborate to provide data with different spatial resolutions or time availability. Moreover, potential applications may also include affordable ground-deployed sensors that can be read from long distances by various space and aerial platforms and V2X systems for communication with fast moving objects or vehicles.

1 INTRODUCTION

Recently, we have observed a growing demand for providing large amounts of data from airborne or space platforms to support and complement existing terrestrial infrastructure services in such application areas as agriculture, automotive, security and production, to name a few. High-speed data transmission is one of the biggest challenges in all these areas as some of the services rely on video, images or hyperspectral data processing that has an impact on antenna systems which are used in point-to-point communication of small and nano-satellite platforms (e.g. CubeSat) but also in other available aerial platforms such as unmanned aerial vehicles (UAVs) or high altitude pseudo-satellites (HAPS). Such platforms using hyperspectral imaging can be effectively used e.g. in better optimization of agriculture processes, which paves the way for precision farming applications [1]. However, to complement hyperspectral imaging with the possibility of monitoring additional soil parameters which cannot easily be acquired using hyperspectral sensors or cameras, it is possible to use dedicated internet of things (IoT) sensors that can be deployed within the area of interest [2], [3]. In future precision farming applications, information acquired from available aerial platforms will be merged because satellites, UAVs and HAPS differ in imaging spatial accuracy and possible revisit times [1], [4] due to their operating altitude. It means that in order to provide affordable sensors that

can seamlessly be read from long distances by different aerial platforms, one has to provide simple and inexpensive in mass production high gain circularly polarized antennas that may be a part of low-cost and energy-efficient soil IoT sensors.

By using circularly polarized (CP) antennas in the communication system, better connection quality can be maintained when the orientation of a transmitting antenna changes towards a receiving antenna. Furthermore, in satellite systems circular polarization plays a significant role in reducing the impact of the Faraday effect. In general, CP wave can be produced by excitation of two orthogonal antenna modes with equal amplitude and a 90° phase shift. However, there are various specific techniques to achieve circular polarization. In microstrip patch, CP wave can be generated by using dual feed technique [5], inserting slot in single-feed patch [6] or using appropriate shapes of patch and truncation [7].

An approach consisting in placing an additional superstrate layer above a microstrip patch apart from effectively increasing the antenna gain, can also be applied to enhance other aspects of the antenna. Such an additional layer, which contain a set of metallic parasitic elements that introduce certain reflections, is commonly described as partially reflecting surface (PRS) [8]-[12]. Such antennas have compact size compared to traditional bulky array antennas. Moreover, PRS antennas provide higher efficiency than traditional arrays because they do not need complex feeding networks.

This paper presents the physical implementation of high gain right-handed circularly polarized (RHCP) superstrate antenna in two different frequency bands typically used in satellite applications. The most significant criteria selected for this investigation are the lowest possible axial ratio (AR) and the highest gain of the antenna in the considered frequency bands and also dimensions not exceeding the Cubesat 1U module size. The measurement results of the presented prototypes are consistent with the simulation results and are also included in this paper.

2 ANTENNA CONCEPT AND DESIGN

The proposed design of high gain circularly polarized antenna with a superstrate layer is based on PRS antenna design presented in Figure 1. The antenna structure contains three separate planar layers, i.e. feeding part with a ground plane, radiating part and a parasitic part called partially reflective surface, which are separated by two air gaps. The highest gain can be obtained for the distance between PRS and the ground plane approximately equal to the half wavelength. Consequently, in such arrangement, it is possible to achieve phase alignment of rays passing through the PRS layer, which results in directivity improvement of the antenna. Because the properties of such an antenna strictly depend on the PRS layer reflection coefficient, the key material parameters affecting the antenna performance are dielectric permittivity and thickness. The placement of metallized passive elements at the bottom of the layer can also have significant impact on the PRS reflection coefficient.

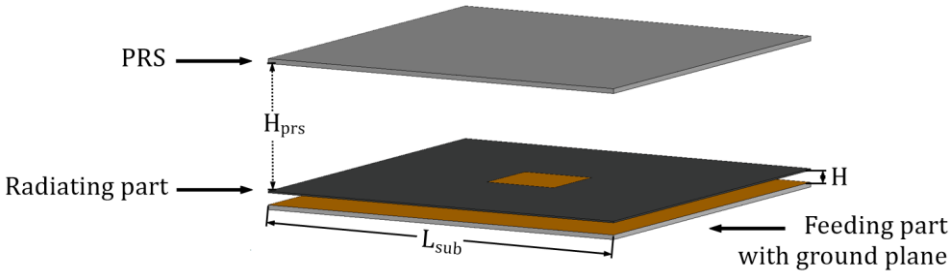

Figure 1. Geometry of the PRS antenna

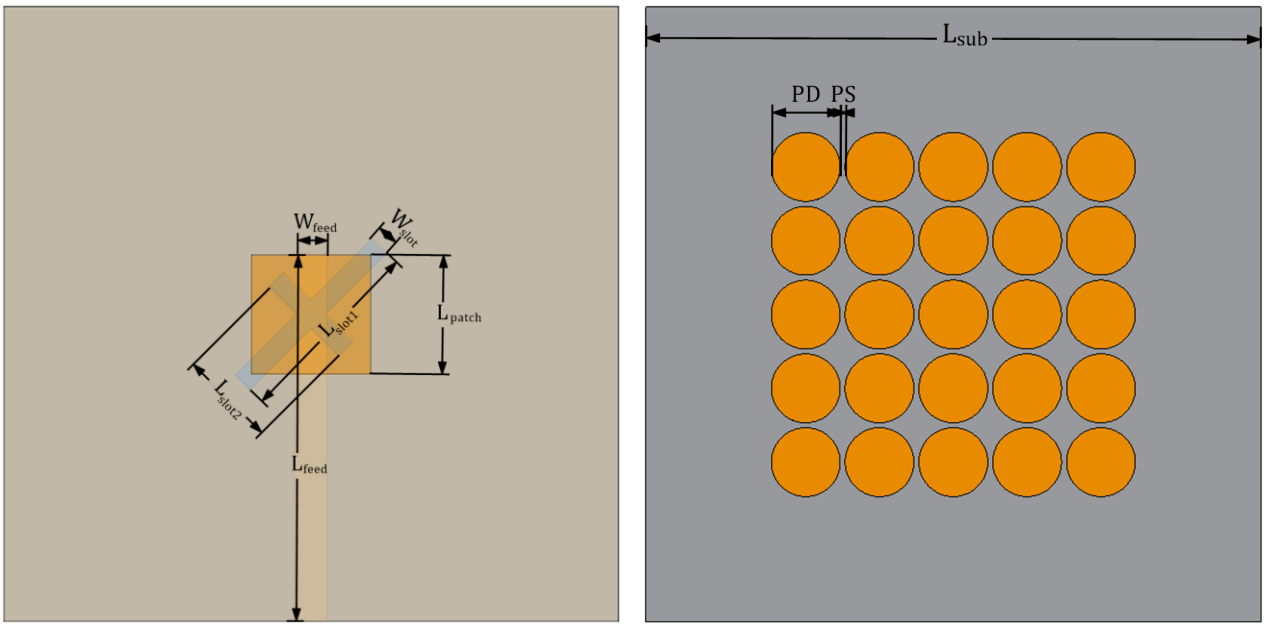

(a) (b)

Figure 2. Geometry of the radiating element (a) and exemplary *5 x 5* PRS structure (b).

2.1 X-band PRS antenna

The X-band PRS antenna was designed at the center frequency of 8.0 GHz. The choice of the radiating element depends on the assumed requirements e.g. bandwidth or type of polarization. In this study, to generate circular polarization (CP), a rectangular patch with the side length of L_{patch} is excited through an *x*-shaped coupling aperture with arms of length L_{slot1} and L_{slot2} spaced at an angle of 90˚ which introduces the appropriate phase shift between modes. This feeding method, apart from wide bandwidth and circular polarization, also ensures mechanical stability of the feeding connector. The coupling aperture is placed in the center of the ground plane on the top side of a thin dielectric layer. On the bottom side of the layer, there is a feed microstrip line with L_{feed} length and W_{feed} width that can be used to easy control the impedance matching. The coupling aperture is skewed by 45˚ relative to the feeding line as presented in Figure 2(a). The feeding line and ground plane with the slot were realized at 0.762 mm thick RO3003 with relative permittivity of 3.0 and loss tangent of 0.001. The second layer in a distance *H* from the ground plane, contains radiating patch placed centrally above the coupling aperture. This layer was designed using 0.254 mm CuClad217 laminate with relative permittivity of 2.17 and loss tangent of 0.0009. The patch itself designed in this way provides a gain of about 7-8 dBi.

An additional dielectric layer with a set of circular passive patches can be applied to improve directional properties. By using materials of different relative permittivity and thickness or applying different sizes or shapes of the conductive passive patches, one can affect the reflection coefficient of the layer and thus control phase alignment of the wave passing through this layer. Such dependence may include such parameters of the antenna as gain, beamwidth or side lobe level (SLL). In the proposed design, the superstrate layer is implemented on 0.787 mm RT/duroid5880 laminate with relative permittivity of 2.2 and loss tangent of 0.0009. Between the source part and the superstrate layer, there is an air gap with the height of H_{prs}. An exemplary passive elements arrangement is presented in Figure 2(b). To facilitate the analysis, this investigation refers to the antenna structures containing an arrangement of all passive elements having the same shape and size. The detailed dimensions of investigated antenna structures for X band were indexed in Table 1. All the presented antenna structures have been designed and simulated using Altair Feko software.

Table 1. Detailed dimensions of X-band antenna

Parameter	L_{feed}	W_{feed}	L_{slot1}	L_{slot2}	W_{slot}	L_{patch}	PD	PS	H_{prs}	H	L_{sub}
Value [mm] 49 passive elements (*7 x 7*)	47.8	1.7	14.5	7.6	1.7	12.5	9.8	0.4	20.1	2	90
Value [mm] 25 passive elements (*5 x 5*)	35.3	1.5	16.7	7.6	1.7	12.5	9.8	0.4	21	2	65

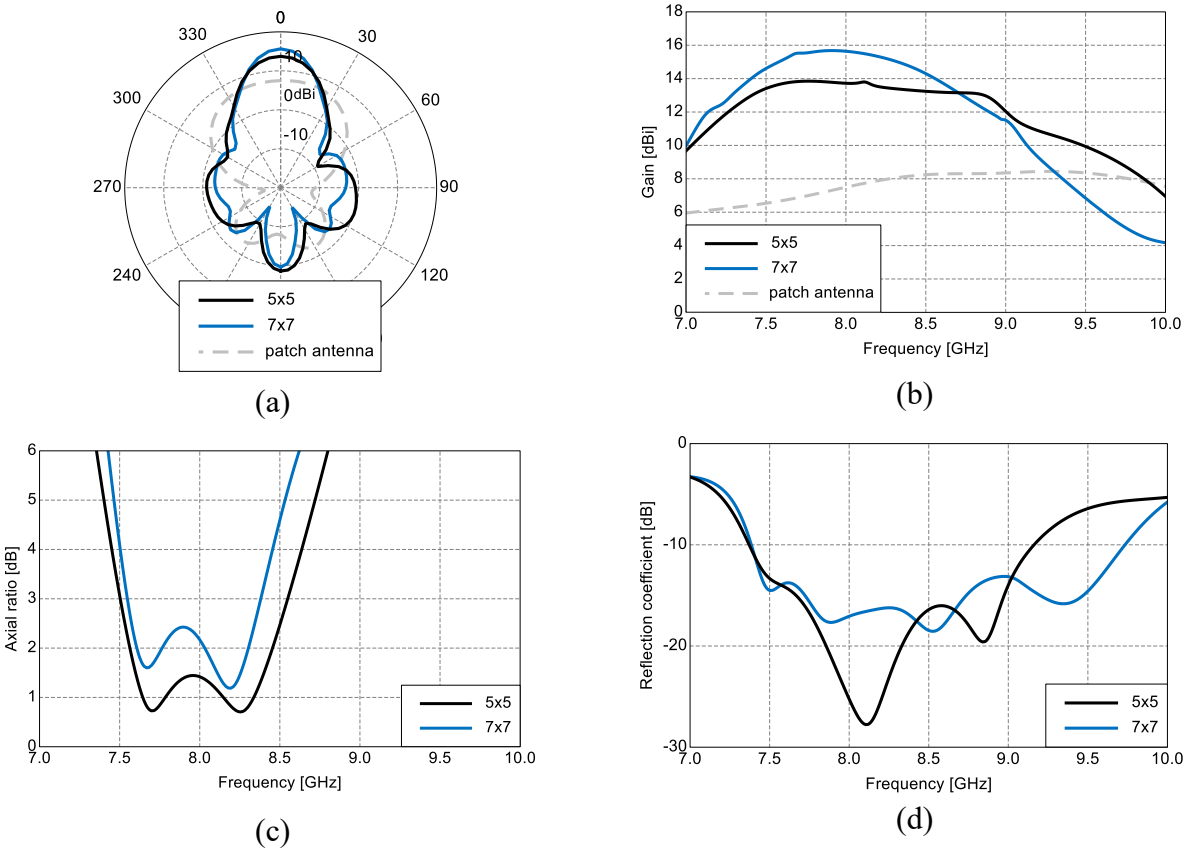

Figure 3. Simulated results of X-band antenna in two versions of PRS – *5 x 5* and *7 x 7*: radiation pattern @8 GHz (φ=0°) (a) , Gain (b), Axial Ratio (c), reflection coefficient (d).

By focusing the analysis only on PRS patterns with an odd number of elements in a row of the array, an additional single row of patches outside the array can be introduced without changing the internal array structure. According to the simulation results of the proposed antenna and its variant with larger number of passive elements, presented in Figure 3, both designs meet the criteria of axial ratio (AR) level below 3 dB and impedance matching (S11 below -10 dB) in a wide frequency range. Larger number of elements results in better beam focusing implying higher gain of the antenna (15.7 dBi and 13.8 dBi for *7 x 7* and *5 x 5* arrangement respectively), nonetheless in both cases, the gain is significantly higher than the patch antenna. Despite the higher gain, the antenna with *7 x 7* arrangement, which almost doubles the number of passive elements compared to the smaller *5 x 5* array, provides slightly lower 3-dB AR bandwidth. The simulation results are collected in Table 2. In order to place a larger array of passive elements on the superstrate layer, it is also necessary to extend the overall dimensions of the antenna to at least 85 mm *x* 85 mm.

Table 2. Specification of X-band antenna

PRS structure size	49 passive elements *(7 x 7)*	25 passive elements *(5 x 5)*
AR 3 dB bandwidth [MHz]	835 (10.4%)	1044 (13.0%)
Maximum gain [dBic]	15.7	13.8
HPBW @8GHz [°]	24.5	31.4
F/B Ratio @8GHz	15.3	12.3
Efficiency [%]	92	95

2.2 X-band *5 x 5* PRS antenna fabrication and measurement results

Our X-band PRS antenna was fabricated in the configuration with *5 x 5* passive element array due to its small overall dimensions. The measured S11 of X-band antenna is presented in Figure 4. The -10 dB bandwidth covers the frequency range from 7.35 GHz to 9.15 GHz. The comparison of the normalized radiation pattern and AR level of measurement and simulation results are presented in Figure 5 and Figure 6 respectively. The presented characteristics confirm the beam-focusing ability of such a superstrate layer narrowing the beam from 80 degrees for a bare patch antenna without superstrate layer about to 31.5 degrees after the addition of the superstrate layer. The AR remains around 3 dB, which confirms the proper circular polarization of the antenna.

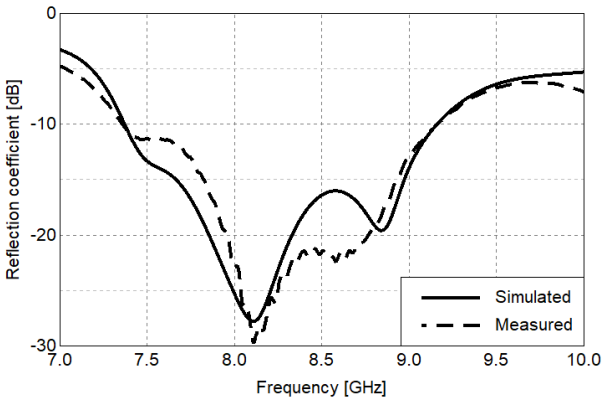

Figure 4. Simulated and measured reflection coefficient results of proposed X-band superstrate antenna

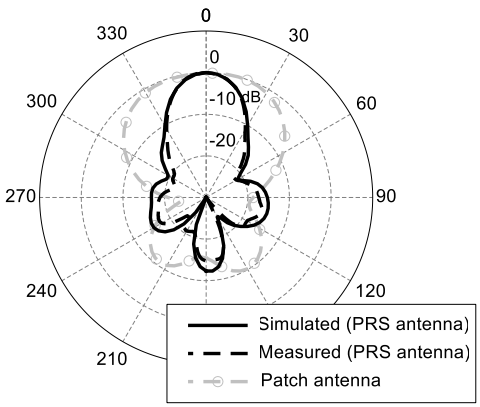

Figure 5. Simulated and measured normalized radiation pattern results of proposed X-band superstrate antenna @8GHz (φ=0°)

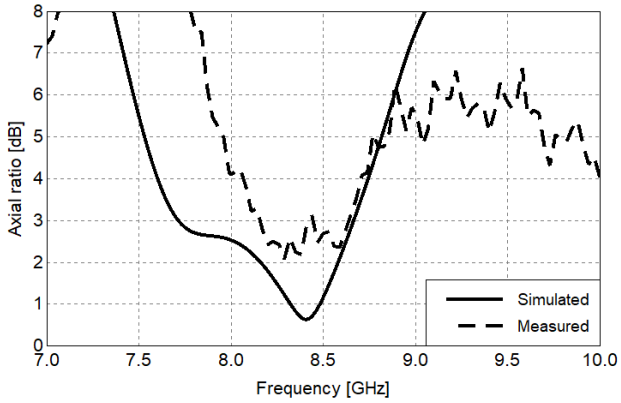

Figure 6. Simulated and measured Axial Ratio results of proposed X-band superstrate antenna

Table 3. Detailed dimensions of Ka-band antenna

Parameter	L_{feed}	W_{feed}	L_{slot1}	L_{slot2}	W_{slot}	L_{patch}	PD	PS	H_{prs}	H	L_{sub}
Value [mm] 81 passive elements (*9 x 9*)	20.8	1.2	4.1	2.55	0.5	2.55	2.8	0.2	5.25	0.6	40
Value [mm] 49 passive elements (*7 x 7*)	16.4	1.24	4.1	2.5	0.5	2.9	2.8	0.2	5.55	0.6	30
Value [mm] 25 passive elements (*5 x 5*)	16.3	1.3	4.2	2.6	0.5	2.9	2.8	0.2	5.75	0.6	30

Table 4. Specification of Ka-band antenna (simulation results)

PRS structure size	81 passive elements (*9 x 9*)	49 passive elements (*7 x 7*)	25 passive elements (*5 x 5*)
AR 3 dB bandwidth [MHz]	2550 (9.3%)	3280 (11.9%)	3660 (13.3%)
Maximum gain [dBic]	14.4	14.4	13.8
HPBW @27.5 GHz	25.8	22.3	28.6
Efficiency [%]	92	94	94
SLL [dB] @27.5 GHz	14.2	11.8	11.4

2.3 Ka-band PRS antenna

Correspondingly to the previous arrangements, similar designs of high-gain antennas were created for the Ka band at the center frequency of 27.5 GHz. Due to smaller overall dimensions of the antenna, a higher order of the passive array than in the case of the X-band antenna was also considered, i.e. array with 81 passive elements in *9 x 9* arrangement. The feeding part with the ground plane and superstrate layer was designed using RT/duroid 5880 with a thickness of 0.787 mm and

CuClad217 with a thickness of 0.254 mm was used for the layer with the radiating patch. The feeding part comprising the ground plane was implemented using a substrate of lower permittivity than in the X-band antenna due to much shorter wavelength at Ka-band frequencies. Each of the proposed designs was tuned taking into particular account the 3-dB AR bandwidth. The detailed dimensions of the proposed antennas are as listed in Table 3.

In Figure 7, the simulation results of the antenna designs for Ka-band are presented. The half-power beamwidth (HPWB) can be easily controlled by the overall size of the array, the size of a single passive cell or the distance of the PRS layer from the radiating patch. However, an array with a large number of passive elements may also increase the level of undesired side lobes. As it is shown in Table 4, increasing the number of passive elements does not improve the gain and even results in a narrower bandwidth. Thus, the *7 x 7* passive elements variant can be considered as the optimal array design, therefore, the fabrication details and measurement results for this particular configuration are discussed in the following section.

2.4 Ka-band *7 x 7* PRS antenna fabrication and measurement results

The proposed antenna with a *7 x 7* array of passive elements has been fabricated and its dimensions are presented in the Table 3. The measured reflection coefficient of the antenna is shown in Figure 8. The minimum is not as deep and -10 dB bandwidth is narrower than the simulation results, but it sufficiently covers the intended satellite frequency bandwidth from 27 to 28.5 GHz. The difference is caused by the insufficient height of the air gap between the layers in the feeding network which is difficult to implement accurately due to its small size in the Ka band. This effect can be mitigated by removing the inter-layer gap and according tuning of the antenna. The radiation pattern of the antenna was measured in a millimeter-wave anechoic chamber. The normalized radiation pattern at 27.5 GHz

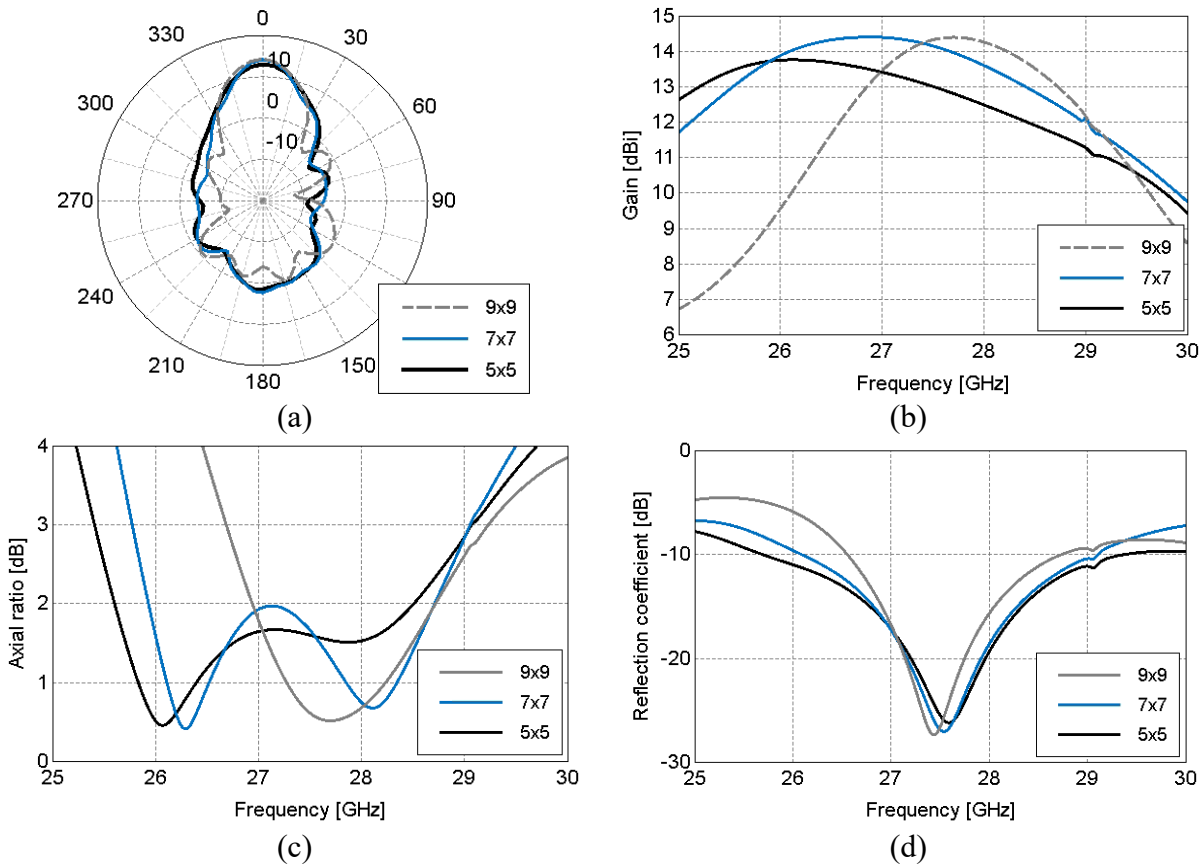

Figure 7. Simulated results of Ka-band antenna in three versions of PRS – *5 x 5*, *7 x 7* and *9 x 9*: radiation pattern @27.5 GHz (φ=0°) (a), Axial Ratio (b), reflection coefficient (c).

compared with the simulation results is shown in Figure 9. In Figure 10, one can see that the CP requirement of AR below 3 dB is fulfilled in a wide frequency band. The narrower AR bandwidth than obtained from the simulations may also be caused by the aforementioned air gap.

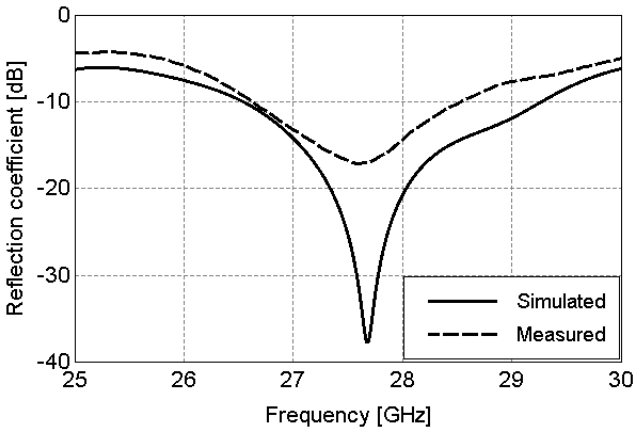

Figure 8. Simulated and measured reflection coefficient results of proposed Ka-band superstrate antenna

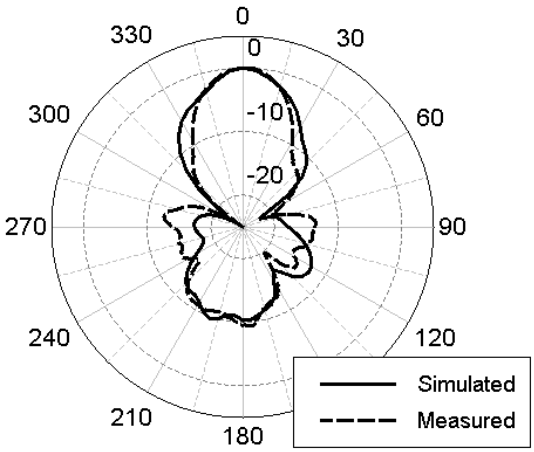

Figure 9. Simulated and measured normalized radiation pattern results of proposed Ka-band superstrate antenna @27.5GHz (φ=0°)

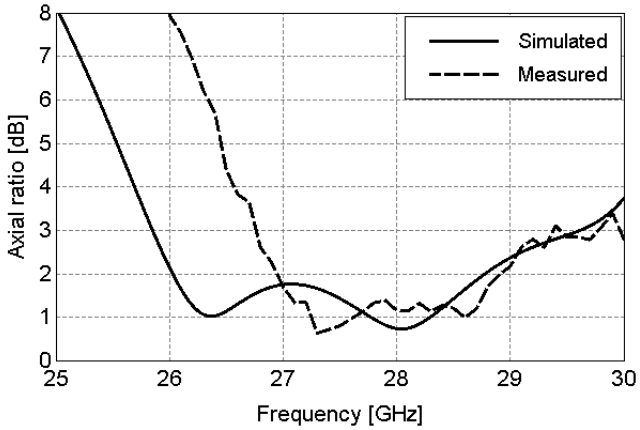

Figure 10. Simulated and measured Axial Ratio results of proposed Ka-band superstrate antenna

3 CONCLUSIONS

In this paper, high gain superstrate antenna with circular polarization for point-to-point communication in aerospace application platforms such as CubeSats, UAVs or HAPS is presented. The antenna was implemented in two frequencies. First, the X-band antenna was designed and then it was investigated whether such an antenna could be easily transformed to a higher Ka-band. In this study, such aspects as circular polarization in a wide band and high gain obtained with the smallest possible total dimensions and weight of the antenna were taken into account. In the presented antenna design, the choice of antenna configuration is a trade-off mainly between the antenna gain and the antenna size in cross-section parallel to the side of the CubeSat and thus it can be easily adapted to the rest of the CubeSat's payload. In the presented prototyped examples, the antenna gain above 13 dBi was achieved in all antenna configurations. The total size of the antenna is 65 *x* 65 *x* 23 mm and 30 *x* 30 *x* 7 mm for X and Ka bands, respectively. The measurement verification confirms that presented type of antenna can work in both frequency bands efficiently and it is easily scalable. Some manufacturing inaccuracies that occurred in fabrication of the prototypes have not affected the operation of the antennas. The development work on this antenna designs can involve more expensive and durable materials and also creating a more compact and mechanically strengthened structure, suitable for placement in a small satellite. There are also a few possibilities of miniaturization of the presented antenna, which will be taken into consideration in our future works.

ACKNOWLEDGEMENTS

This paper is a result of the BEYOND5 (www.beyond5.eu) project which has received funding from the ECSEL Joint Undertaking (JU) under grant agreement No 876124. The JU receives support from the European Union's Horizon 2020 research and innovation programme and France, Germany, Turkey, Sweden, Belgium, Poland, Netherland, Israel, Switzerland, Romania. The document reflects only the authors view and the Commission is not responsible for any use that may be made of the information it contains. This work was also partially supported by Polish Ministry of Science and Higher Education grant for statutory activities at Faculty of ETI, Gdansk University of Technology.

4 REFERENCES

[1] I. Bhakta, S. Phadikar, K. Majumder, "Stateoftheart technologies in precision agriculture: a systematic review", Journal of the Science of Food and Agriculture, vol. 99, pp. 4878, 2019.
[2] R. Müller, J. J. Kiam and F. Mothes, "Multiphysical simulation of a semi-autonomous solar powered high altitude pseudo-satellite," 2018 IEEE Aerospace Conference, Big Sky, MT, 2018, pp. 1-16.
[3] A. M. Ezhilazhahi and P. T. V. Bhuvaneswari, "IoT enabled plant soil moisture monitoring using wireless sensor networks," 2017 Third International Conference on Sensing, Signal Processing and Security (ICSSS), Chennai, 2017, pp. 345-349.
[4] P. Horstrand, R. Guerra, A. Rodríguez, M. Díaz, S. López and J. F. López, "A UAV Platform Based on a Hyperspectral Sensor for Image Capturing and On-Board Processing," in IEEE Access, vol. 7, pp. 66919-66938, 2019.
[5] K. N. Khac et al., "A Design of Circularly Polarized Array Antenna for X-Band CubeSat Satellite Communication," 2018 International Conference on Advanced Technologies for Communications (ATC), Ho Chi Minh City, 2018, pp. 53-56.
[6] Jui-Han Lu, Chia-Luan Tang and Kin-Lu Wong, "Single-feed slotted equilateral-triangular microstrip antenna for circular polarization," in IEEE Transactions on Antennas and Propagation, vol. 47, no. 7, pp. 1174-1178, July 1999.

[7] F. Kurniawan, J. T. S. Sumantyo, Mujtahid and A. Munir, "Effect of truncation shape against axial ratio of left-handed circularly polarized X-band antenna," 2017 15th International Conference on Quality in Research (QiR) : International Symposium on Electrical and Computer Engineering, Nusa Dua, 2017, pp. 83-86.
[8] L. Leszkowska, M. Rzymowski, K. Nyka and L. Kulas, "High-Gain Compact Circularly Polarized X-Band Superstrate Antenna for CubeSat Applications," in IEEE Antennas and Wireless Propagation Letters, vol. 20, no. 11, pp. 2090-2094, Nov. 2021.
[9] Mousavi Razi, Zahra & Rezaei, Pejman. (2013). Fabry Perot Cavity Antenna Based on Capacitive Loaded Strips Superstrate for X-Band Satellite Communication. Advanced Radar Systems Journal. 2. 26-30.
[10] Z. Wu, L. Li, Y. Li and X. Chen, "Metasurface Superstrate Antenna With Wideband Circular Polarization for Satellite Communication Application," in IEEE Antennas and Wireless Propagation Letters, vol. 15, pp. 374-377, 2016.
[11] G. Ganaraj, C. Kumar, V. S. Kumar and Shankaraiah, "High gain circularly polarized resonance cavity antenna at X-band," 2017 IEEE International Conference on Antenna Innovations & Modern Technologies for Ground, Aircraft and Satellite Applications (iAIM), Bangalore, 2017, pp. 1-5.
[12] G. V. Trentini, "Partially reflecting sheet arrays," in IRE Transactions on Antennas and Propagation, vol. 4, no. 4, pp. 666-671, October 1956.